

Memo on the Evaluation of Downscaled GCMs Using WRF

Prepared by Stefan Rahimi, UCLA
October, 2022

- This research is funded by the California Energy Commission (CEC) through its Electric Program Investment Charge (EPIC) Program, which invests in scientific and technological research to accelerate the transformation of the electricity sector to meet the state's energy and climate goals.
- The research project, EPC-20-006, will integrate the latest downscaling approaches applied to the recently produced global climate models (GCMs) with an engagement process to develop a robust, usable, set of climate projections applicable for California.
- This memo and data here within are being shared to support transparent and timely consideration of interim deliverables that are relevant for energy stakeholders and all those interested in California's next generation of climate projections. The memo does include data that was part of non-CEC leveraged projects.

This memorandum is submitted to the CEC by UC San Diego's Scripps Institution of Oceanography. The report meets deliverable requirements under Task 4 of the California Energy Commission's Project EPC-20-006: Development of Climate Projections for California and Identification of Priority Projections.

Synopsis

In this document, we evaluate the performance of a developing suite of dynamically downscaled global climate models (GCMs) with emphasis on four projections as part of EPC-20-006, Task 4. Specifically, GCMs from the 6th Coupled Model Intercomparison Project (CMIP6) are downscaled here using the Weather Research and Forecasting (WRF) model. More information on the development of these 4 dynamically downscaled projections can be found in the *Memo on the Development and Availability of Dynamically Downscaled Projections Using WRF* - another Task 4 deliverable of the California Energy Commission's Project EPC-20-006. The GCMs that were dynamically downscaled were preselected based on their abilities to simulate the atmospheric circulation (both in the Northern Hemisphere and across California), extremes, and California's temperature and precipitation; as well as availability of data at 6-hour intervals on native GCM levels to drive WRF. However, large differences between historical downscaled WRF simulations and observations exist and are discussed in this document. In addition, we highlight the range in results of climate projections from the ensemble of dynamically downscaled models as well as focus in on the effects of a pre-downscaling bias correction of the mean-state fields used to drive WRF.

1. Introduction

Dynamical downscaling is a popular technique used in the synthesis of physically based high-resolution weather and climate projections. Conducted over a limited area of the planet, historical reanalyses are often dynamically downscaled using the Weather Research and Forecasting (WRF; Skamarock et al., 2019) model to reproduce focused landscape-scale atmospheric and surface conditions (Liu et al., 2011, 2017; Rahimi et al., 2022; Rasmussen et al., 2014). The high-resolution output allows us to study weather- and climate-relevant processes that may unfold across sparsely observed regions, gain physical insights into their land-atmosphere drivers, and their high-spatial resolution/frequency outputs can be used to drive land-surface, hydrologic, and fire models. Regional climate models (RCMs) such as WRF are typically designed to downscale reanalysis, as scientists seek to improve their physical solvers and numerics to increase the precision and confidence of forecasts by benchmarking simulation results against historically observed events. Indeed, dynamical downscaling, when implemented properly, may even yield solutions within the bounds of observational uncertainties (Lundquist et al., 2019).

Direct dynamical downscaling of GCMs is far less common than dynamically downscaling reanalyses in regional climate modeling for a variety of reasons but still yields a result based solely on computational physics (Bruyère et al., 2014; Coppola et al., 2020, 2021; Huang et al., 2020; Komurcu et al., 2018; Wang et al., 2016; Wang & Kotamarthi, 2015; Zobel et al., 2017, 2018). Direct dynamical downscaling has important strengths relative to other downscaling methods. For example, dynamical downscaling of GCMs doesn't assume stationarity (Lanzante et al., 2018) in its creation of the high resolution predictands as is the case in other forms of downscaling (e.g., statistical). The dynamically downscaled solution can in fact resolve plausible extreme weather events that may only emerge in an unobserved future (or historical) climate

state. Additionally, RCMs use the primitive governing equations to integrate a diversity of physical quantities that cannot be obtained through statistical methods or via machine learning techniques owing to lacking observations and subsequent training data. For example, statistically downscaled precipitation and temperature, even when obtained using multivariate relationships, may contain no information about water vapor content, surface pressure, cloud depth, etc. Finally, and perhaps most fundamentally, the use of physics to arrive at the downscaled result means that physically interpretable feedbacks between the landscape and the overlying atmosphere can be interactively simulated. Despite these strengths, however, dynamical downscaling must be applied with caution owing to large biases within the driving GCMs which may be propagated to and amplified by an RCM's physical solvers during downscaling, and these biases should be dealt with via the use of bias correction.

Additionally, barriers to using RCMs to dynamically downscale GCMs exist because: 1. RCMs rely heavily on the actual data of the GCMs (which may not include all needed/desired variables), 2. RCM configurations may not be designed to ingest GCM data as boundary conditions, and 3. the high computational cost to dynamically downscale GCMs. Because of these barriers, large ensembles of dynamically downscaled landscape-resolving (10 km grid spacing) climate projections generally remain out of reach.

As part of EPC-20-006, we provide a set of four dynamically downscaled GCM projections and a dynamically downscaled reanalysis (Task 4) for use in hybrid downscaling (Task 5) and hydrologic modeling (Task 6) across the western United States (WUS). Specifically, we provide simulations on a convective-permitting grid that covers all of California as well as another suite of 9-km simulations with coverage across 11 WUS states, including the whole of the Western Electricity Coordinating Council (WECC) region. In the following sections, we present an overview of these projections and our methodology, a characterization of their historical performance and future change signal, and a broad comparison to the greater ensemble of which they are a part of. We will also present a high-level summary on how these WRF (dynamically downscaled) projections are to be used within a statistical downscaling framework to develop a hybrid downscaling methodology, as well as serve as input data for the hydrologic simulations also carried out as part of this project.

2. Methodology

The development of high-resolution and physically based climate ensembles presents researchers with some major practical difficulties (the barriers discussed above). We address these difficulties below, and we provide justification for our RCM setup.

2.1 Parallelization approach

WRF simulations are conducted for the period 1 August 1980 through 1 September 2100. We downscale each year of integration separately and in parallel; each model year is initialized to the driving GCM/reanalysis state. In this way, an N -year simulation is completed in the same amount of wall clock time as a 1-year experiment, where N is the total number of years. For each year of integration, we choose the beginning of the retained WRF output to coincide with minimum snowpack across the western United

States (September 1). This approach minimizes the dependence of the simulations on soil moisture and snowpack derived from the previous water year, which is poorly represented by the coarse-resolution driving datasets (GCM or reanalysis). Given that we require 1 month of spin-up, WRF is initialized on August 1 to surface and three-dimensional data from the GCM/reanalysis and integrated through September 1 of the following year (13 months, including the spin-up month) on 39 atmospheric levels. This approach is like Zobel et al. (2017, 2018), who initialized WRF experiments at yearly intervals but only allowed for 1 day of model spin-up.

For the purposes of accurately simulating streamflow, which is a main priority of Task 6, fully time-continuous land-surface simulations need to be conducted. This is because soil moisture/temperature conditions may take years to properly equilibrate to the local weather, and these soil properties have a large impact on subsequent streamflow. WRF's parallelization procedure, which is advantageous for executing simulations in weeks instead of years, is performed to the detriment of time continuity in simulating the surface and subsurface runoff with high precision. To address the issue of continuity in simulating streamflow for Task 6, atmospheric fields from WRF, which are of high accuracy, are used to drive offline hydrology models that are continuous (such as WRF-Hydro and VIC used in Task 6).

2.2 Model options, grid, and physics

Our final model setup, applied to the reanalysis-driven and all GCM-driven simulations, was informed through the results of 21 year-long sensitivity experiments overviewed in Rahimi et al. (2022). Superficially, these test experiments examined the result sensitivity to user choices in spectral nudging strength, microphysics and cumulus parameterization choices, land surface model solver choices, and reanalysis choice. We conducted these experiments because large dry biases in snow water equivalent and precipitation were found when we used parameterizations based on recently published WRF studies across the WUS, which is the focus region for this work. For a more quantitative overview of our testing procedure, see section 2 of Rahimi et al. (2022). We assert that extensive testing over the complete annual cycle is generally a best practice when trying to identify a set of model parameterizations/solvers across a focus region prior to downscaling over a climatology period.

In our finalized WRF setup, we dynamically downscale all simulations to a 45-km grid on which the horizontal winds, temperature, and geopotential height are relaxed to their respective reanalysis/GCM-simulated fields via spectral nudging for wavelengths greater than 1,500 km in length above the planetary boundary layer; smaller waveforms were allowed to evolve freely on the WRF grid. One-way nesting is then used to dynamically downscale the 45-km result to a 9-km grid on which spectral nudging is not implemented. Specifically, output from the 45-km simulations provides the lateral boundary conditions for the 9-km experiments. Finally, we one-way nest from 9- to 3-km without spectral nudging. All grids are shown in Figure 1. The lateral boundary conditions are updated at 6-hourly intervals, and adaptive time stepping is used. On the 45- and 9-km grids, convective precipitation is parameterized following Tiedtke (1989) and Zhang et al. (2011); the cumulus scheme is disabled in the 3-km experiments which

are assumed to be convective permitting. P3 microphysics is used (Morrison & Milbrandt, 2015), shortwave and longwave radiation schemes of Iacono et al. (2008) are implemented, and the Noah land surface model with multiparameterizations (Noah-MP) is used (Niu et al., 2011).

2.3 Reanalysis-driven experiment

As informed by model testing, we dynamically downscaled the European Centre for Medium-range Weather Forecasting's fifth Reanalysis (ERA5; Hersbach et al., 2020) from 1 September 1980 to 31 August 2020 as described in Rahimi et al. (2022). For purposes of this project we also dynamically downscaled ERA5 from 1 September 1950 through 31 August 1980 and from 1 September 2020 through 31 August 2021 to provide a 70-year downscaled reanalysis from 1950 through 2021. While a general characterization of biases in the 40-year downscaled reanalysis is presented in Rahimi et al. (2022) below we advertise the full 70-year downscaled product, named ERA5, as we assess biases in dynamically downscaled GCMs.

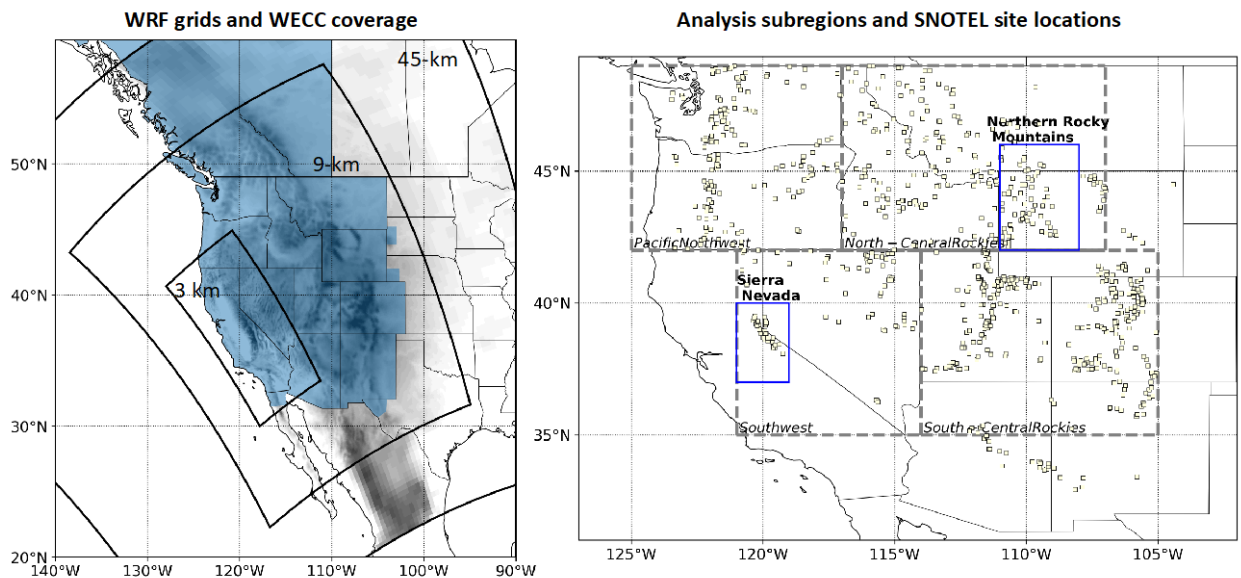


Figure 1. The pane on the left shows the WRF grids with shaded topography, while the Western Electricity Coordinating Council (WECC) region is shaded in blue. The right pane shows our analysis subregions (dashed lines) for WRF comparisons to SNOw TELemetry sites (black boxes).

2.4 GCM-driven experiments

Next, we dynamically downscale four CMIP6 GCMs from 1980 to 2100. These GCMs were selected because, at the time of selection, of the GCMs with the requisite data to drive WRF, they exhibited the most skill compared to other CMIP6 GCMs. The GCM selection process is described in the, *Memorandum on Evaluating Global Climate Models for Studying Regional Climate Change in California* an interim deliverable for

this project's task 3. As mentioned previously, computational limitations preclude our team from dynamically downscaling more GCMs to the 3-km California grid under this project; however, many more GCMs are currently being downscaled to 9-km across the western United States with funding from other sources.

To account for the impacts of greenhouse gases on the model energetics, updating annual and Northern Hemispheric mean CMIP6 historical carbon dioxide and methane concentrations are used in WRF's longwave radiation scheme from 1980-2014, while anthropogenic emissions from the third Shared Socioeconomic Pathway (SSP3) with an end-century top-of-the-atmosphere radiative forcing of 7 W m^{-2} is (SSP3-7.0) are used from 2014 to 2100. Table 1 shows a list of the GCMs provided to this project (EPC-20-006).

Table 1. Listing of dynamically downscaled CMIP6 GCMs provided under EPC-20-006. The GCM resolutions are approximate since many CMIP6 GCMs have stretched horizontal grids near the poles (e.g., FGOALS-g3).

	GCM	Modeling center	SSP	Variant	WRF grids	GCM resolution (latitude/longitude)	Abbreviation
1	CESM2	NCAR	3-7.0	r11i1p1f1	45,9,3	$0.94^{\circ} \times 1.25^{\circ}$	CESM2
2	CNRM-ESM2-1	CNRM-CERFACS	3-7.0	r11i1p1f2	45,9,3	$1.4^{\circ} \times 1.4^{\circ}$	CNRM
3	EC-Earth3-Veg	EC-Earth Consortium	3-7.0	r11i1p1f1	45,9,3	$0.7^{\circ} \times 0.7^{\circ}$	ECE
4	FGOALS-g3	CAS	3-7.0	r11i1p1f1	45,9,3	$2.1^{\circ} \times 2.0^{\circ}$	FGOALS

Modeling centers report many more results on isobaric surfaces versus native model levels in CMIP6 given the much smaller data volume of the former. In WRF, a sufficiently high vertical resolution is recommended to force the model. Additionally, 6-hourly forcing updates are generally recommended, but most modeling centers do not report the requisite 6-hourly data to drive WRF, although many do report daily data. To increase the number of potential downscalable GCMs, our team conducted tests in which (i) data on a mere 6 pressure levels was used to drive WRF and (ii) a daily forcing interval was used. In both instances, large differences between the control (forced with 6-hourly data on 25 isobaric surfaces) and the two test cases were noted, forcing us to proceed adherent to WRF's best practices.

2.5 Sea surface temperatures

Sea surface temperatures (SSTs) are prescribed to update daily in WRF to the reanalysis/GCM values, except for the Flexible Global Ocean-Atmosphere-Land System (FGOALS) which only contained monthly SST output in downscaling. For FGOALS, linear interpolation was used to upsample monthly SST means, valid at the midpoint of each month, to daily values.

SST warmth in the Gulf of California (GoC) is known to have a strong impact on the North American Monsoon, which provides roughly a third of Arizona and New Mexico’s annual precipitation (Mitchell et al., 2002). As downscaling progressed, we began to consider the consequences of the fact that the GoC is not resolved in CMIP6 GCMs because of their coarse resolutions. As a result, there is no SST information from GCMs across the GoC that can be used to directly prescribe SSTs in the WRF-resolved GoC. For CESM2 and CNRM, GoC SSTs were extrapolated from the adjacent Pacific SSTs. However, the SST climatologies of the open Pacific (directly west of the California Sur) and the GoC can be vastly different; specifically, the open Pacific SSTs are cooler and exhibit a weaker seasonal variability. Furthermore, we found a strong anticorrelation between the climatological GoC entrance region temperature and the along-axis GoC SST gradient, indicating that we may be able to apply a linear relationship to extrapolate the GoC SSTs. In the GoC, we thus apply the following linear extrapolation,

$$T_{GoC} = \left. \frac{\partial T}{\partial n} \right]_{ERA5}(n) + T_{entry,GCM},$$

where $\left. \frac{\partial T}{\partial n} \right]_{ERA5}$ is the monthly varying climatological GoC temperature gradient and is always positive as SSTs are always warmer further south and east, n is the along-GoC axis coordinate, and $T_{entry,GCM}$ is the GoC entrance temperature, which is resolved in GCMs. A schematic showcasing the origins of this relationship is given in Figure 2.

Hence, for EC-Earth3-Veg (ECE) and FGOALS (and 16 of 18 GCMs in the remaining greater ensemble), we applied the above linear extrapolation relating the GoC entrance region meant SST, a feature resolved in all GCMs, to the GoC SSTs by using a monthly varying SST gradient, derived from ERA5 over the 1980-2014 period.

3. Historical performance

We intentionally narrow the scope of our historical analysis to temperature and precipitation for a variety of reasons. Firstly, certain variables such as simulated snow water equivalent, streamflow, and evapotranspiration will be provided to end-users by driving calibrated offline hydrologic simulations (Task 6) using bias corrected WRF-simulated precipitation and temperature as inputs, thus yielding a result more comparable to the observed climatology. Secondly, these variables have high-confidence historical reference datasets available due to sufficient recording of observations. Other variables, such as near-surface wind, do not have this. Third, precipitation and temperature are of fundamental importance to this project’s statistical downscaling and hydrologic modeling teams. Finally, we chose to dynamically downscale CESM2, CNRM, FGOALS, and ECE based on their skill in simulating precipitation and temperature, as well as their future diversity in their changes. Although we assess the skill of the GCMs, the dynamically downscaled GCM results may be largely different than an observed data product owing to (i) internal climate variability differences and (ii) large GCM biases that are propagated into WRF during downscaling, resulting in an amplified bias, even in the GCMs that performed well in the Task 3 evaluation.

We examine California statewide mean biases in the wet season (October through March climatology) and in the warm season (June through September climatology) between 1980 and 2014. Figures 3 and 4 show the historical climatology of wet and warm season 2-m temperature (T2MEAN) amongst the ERA5-driven and GCM-driven experiments, along with a climatology from the Parameter-elevation Regressions on Independent Slopes Model (PRISM; PRISM Climate Group, 2021). PRISM is a commonly used observationally based gridded product that is often used to assess a RCM's skill in predicting temperature and precipitation.

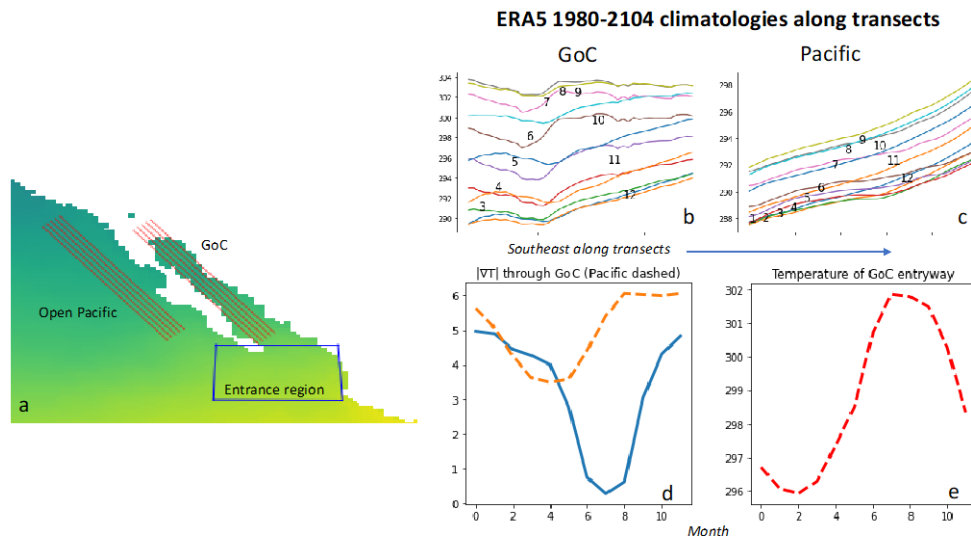


Figure 2. Subpanel (a) shows the coastal geometry from the 30-km-resolution ERA5 product along with 5 transects parallel the coastline within the Gulf of California (GoC) and the Open Pacific. Monthly climatological (1980-2014) temperatures along these transects are shown in panels (b) and (c) respectively; we note large differences in monthly temperature magnitudes and seasonal variability between the two regions, respectively. Subpanel (d) shows the climatological temperature gradient magnitudes for (dashed) the Open Pacific and (solid) the GoC averaged over the 5 transects, respectively. Subpanel (e) shows the climatological GoC Entrance region temperature by month. For panels (d) and (e), the month of January (December) is denoted by 0 (11) on the abscissa.

As expected, the heterogeneity of the WRF result reflects the geographic diversity of California, although the results are characterized by notable biases (Figure 5). During the wet season, an ERA5 warm bias of 1°C is simulated in the Central Valley. Meanwhile, ERA5 can be locally 1-4°C cooler than PRISM across the high Sierra and portions of northern California, although these locations are sparsely observed which raises concerns regarding PRISM's fidelity. This bias profile (warm at low-elevations and cold at higher elevations) is consistent with other studies such as Rahimi et al. (2022) and Liu et al., (2017), the cause of which is actively being researched by WRF developers. For the GCMs, the biases are qualitatively like those in ERA5, with the Central Valley showcasing an even larger warm bias (3°C). CESM2 and ECE (CNRM

and FGOALS) have a smaller (larger) Sierra cold bias than ERA5 during the wet season.

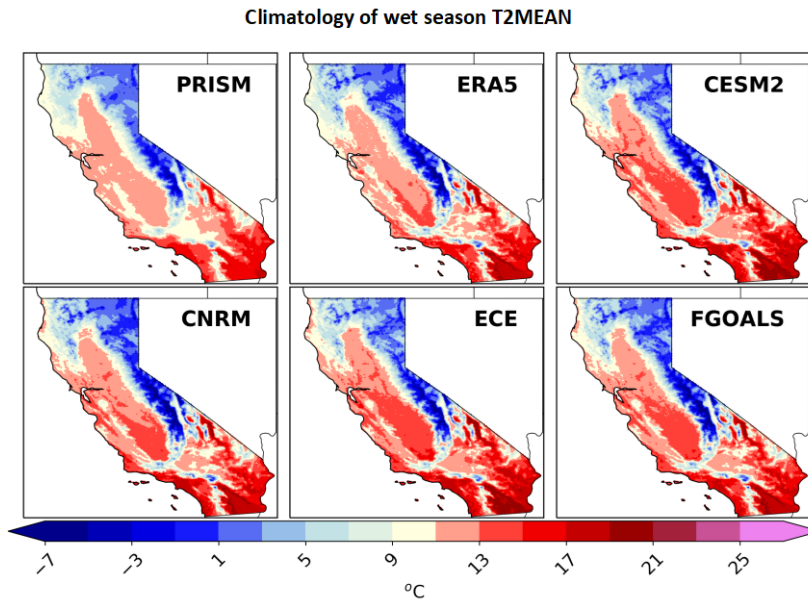


Figure 3. Historical climatology (1980-2014) of wet season (October through March mean) of 2 m temperature (T2MEAN) from 5 dynamically downscaled products at 3 km and PRISM.

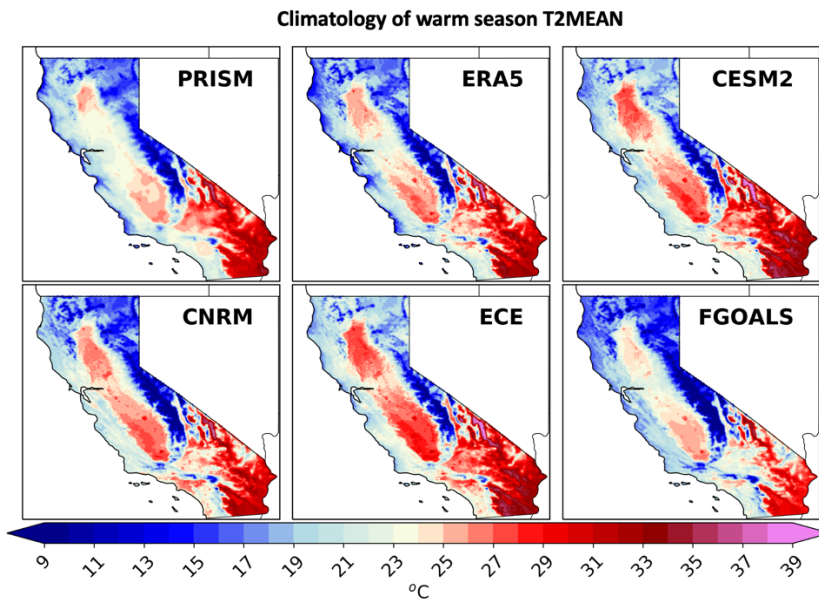


Figure 4. Historical climatology (1980-2014) of warm season (June through September mean) of 2 m temperature (T2MEAN) from 5 dynamically downscaled products at 3 km and PRISM.

During the warm season, the bias pattern is more complex than in the wet season. ERA5 is the least-biased product, again showcasing a cold bias of 1-2°C in the high

Sierra (Fig. 5). ERA5 also exhibits a cold bias of similar magnitude across the northern California coast. On the other hand, CESM and ECE are generally characterized by warm biases almost everywhere in the state, with biases approaching 4°C in portions of the Central Valley and eastern Sierra; biases in these two simulations are minimized across the Sierra and are even smaller than ERA5. CNRM and FGOALS can locally be more than 4°C colder than PRISM along the spine of the Sierra, while CNRM is 3°C warmer than PRISM in the Central Valley. Finally, aside from the Central Valley, FGOALS is 2-5°C cooler than PRISM across portions of northern and southeastern California.

WRF-simulated wet season precipitation (PREC) is expectedly correlated with California’s complex topography (Figure 6), and its biases are more uniform in sign than those of T2MEAN for the downscaled GCMs in that they are almost universally wet (Figure 7). Additionally, the bias magnitudes grow with increasing elevation. ERA5 is by far the most comparable with PRISM with wet biases of 3-4 mm/d at the highest elevations of the high Sierra where confidence in PRISM’s fidelity is reduced. CESM2 and ECE are the least biased GCMs but still see biases that exceed 9 mm/d locally across the high Sierra and across northern California. Like the T2MEAN results, CNRM and FGOALS are the most biased of the four downscaled GCMs for wet season precipitation, with nearly the entirety of the Sierra seeing >10 mm/d more than PRISM over the historical period.

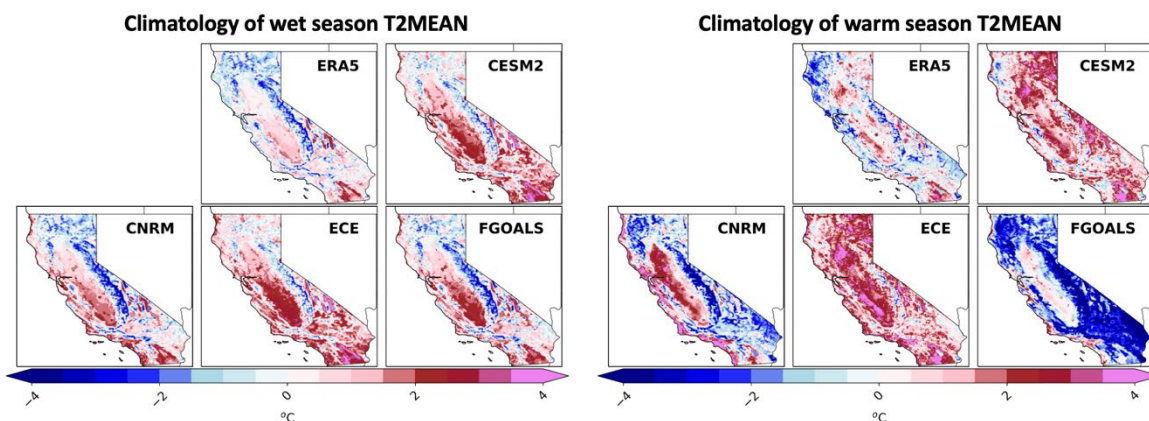


Figure 5. Climatologies of wet (left) and warm (right) season T2MEAN biases amongst the various downscaled products relative to PRISM.

Next, we examine monthly California-mean temperature and precipitation biases by quantile (Figure 8). For T2MEAN, ERA5 most skillfully reproduces the reference quantiles from PRISM; ERA5 in fact exhibits superior performance compared to the GCM simulations for PREC and 2 m maximum temperature (T2MAX). ERA5 biases are constant across quantiles – near zero for T2MEAN and T2MAX and around +2K for 2 m minimum temperature (T2MIN). For PREC ERA5 exhibits a bias of less than 0.2 mm/d that increases to 0.54 mm/d and 0.72 mm/d for the 90th and 95th percentiles, respectively.

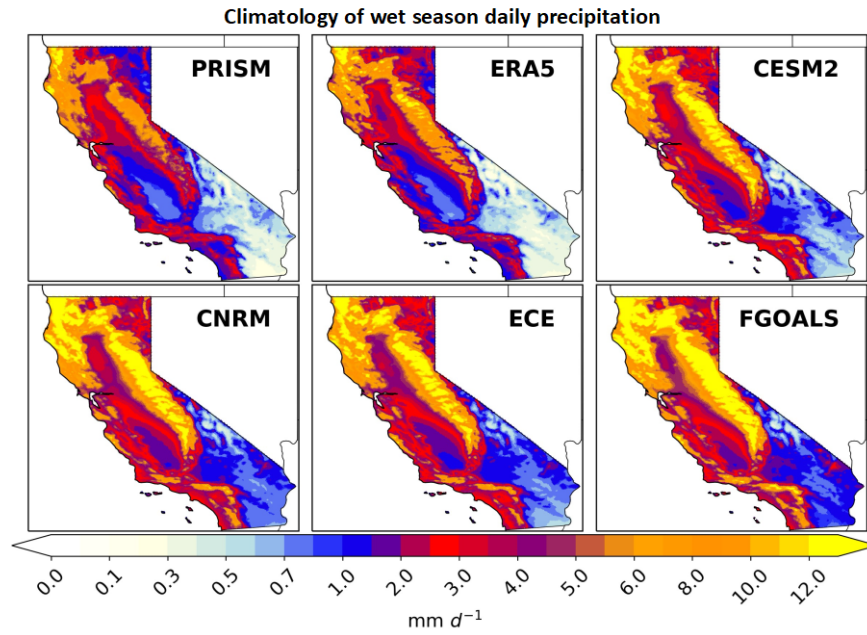


Figure 6. Historical climatology (1980-2014) of wet season (October through March mean) of precipitation (PREC) from 5 dynamically downscaled products at 3 km and PRISM.

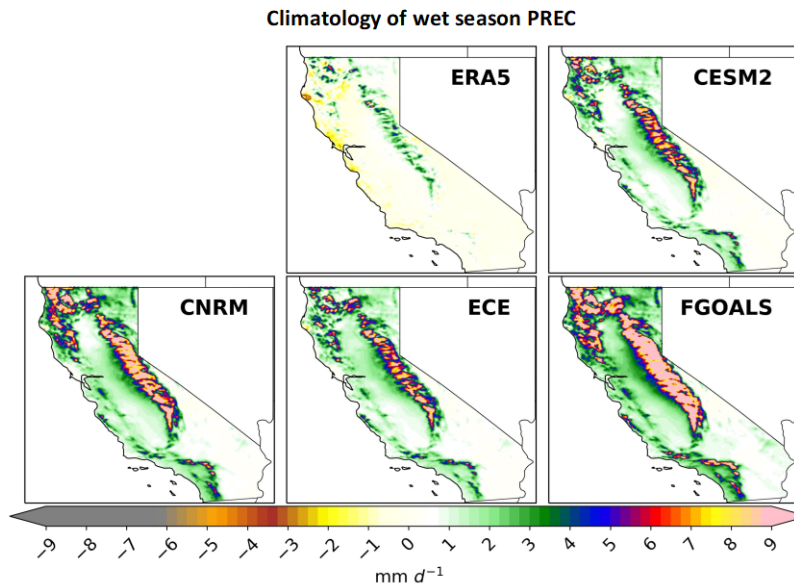


Figure 7. Historical climatology of wet season (October through March) biases in precipitation (PREC).

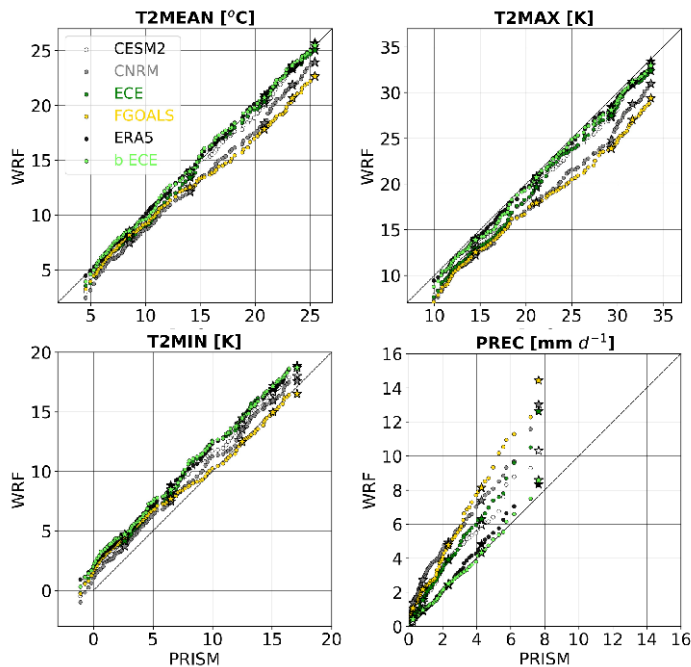


Figure 8. Observed (abscissa) versus WRF-simulated (ordinate) monthly-mean variables by quantile (1st to 99th incremented by 1) for the various downscaled products averaged over California. Quantiles were computed by resampling the daily time series to monthly means and averaging across the entire state of California. The stars denote the 25th, 50th, 75th, 90th, and 99th percentiles, while circles are used for all other quantiles. An additional EC-Earth experiment is presented here, 'b ECE'. This experiment is identical to ECE except that a mean-state bias correction is applied to the GCM inputs prior to downscaling.

When viewed by quantile, the dynamically downscaled GCMs continue to present much larger biases relative to ERA5. It appears all downscaled GCMs have issues with simulating the amplitude of the daily temperature cycle as evidenced by their uniform cold bias in T2MAX and warm bias in T2MIN. FGOALS and CNRM are more biased than CESM2 and ECE for T2MIN, T2MAX, and T2MEAN, while ECE, ERA5, and bias corrected ECE (b ECE; discussed shortly) are minimally biased. Overall, cold biases in T2MEAN are driven by cold biases in T2MAX and is most probably related to wet median precipitation bias of 0.57 mm/d, 1.89 mm/d, 0.73 mm/d, and 1.34 mm/d, in CESM2, CNRM, ECE, and FGOALS, respectively. Magnitudes in PREC biases grow with increasing quantile; the 90th quantile biases are 1.69 mm/d, 3.12 mm/d, 2.03 mm/d, and 3.88 mm/d for CESM2, CNRM, ECE, and FGOALS, respectively. For the 99th percentile, biases of 2.70 mm/d, 5.40 mm/d, 5.00 mm/d, and 6.81 mm/d are simulated for CESM2, CNRM, ECE, and FGOALS, respectively.

We note the minimal biases in b ECE, especially for precipitation, which can even be smaller than those in ERA5; this experiment was conducted following a correction of mean-state biases relative to ERA5 prior to downscaling. The removal of these biases,

which can be quite large (see below), can increase the realism of dynamically downscaled results but may also introduce uncertainty in the dynamically downscaled signal (hence the choice not to use this form of bias correction for EPC-20-006).

While the California-mean biases in temperature and precipitation are remarkably large, they are at least somewhat physically interpretable and consistent with some of the mean-state biases from the parent GCMs that are propagated into WRF during dynamical downscaling. Despite a comprehensive processed-based GCM evaluation prior to downscaling, we found there to be large biases in the climatological mean of certain variables used to drive WRF. Here, we define a mean-state variable by decomposing its full signal into a linear summation of a climatological mean and its deviation from the mean. For example, for temperature T , the decomposition yields $T(x, y, z, t) = \underline{T}(x, y, z) + T'(x, y, z, t)$. \underline{T} is computed over the climatology period (1980-2014), and its bias is found by direct comparisons with ERA5. We show climatological wintertime biases for temperature and zonal wind, averaged over the eastern Pacific and western North America (20° - 55° N and 140° - 90° W area-weighted) in Figure 9.

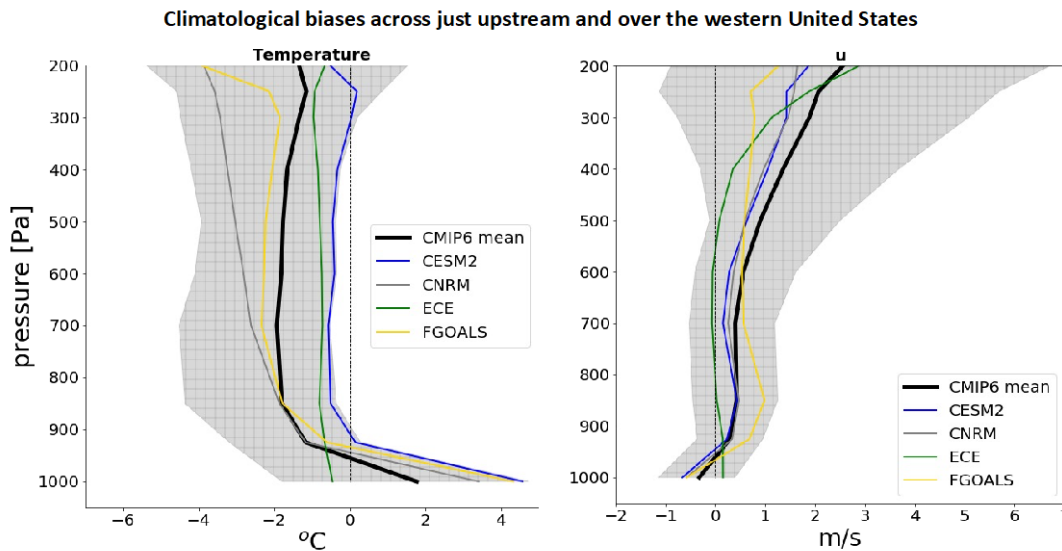


Figure 9. Vertical profiles of historical (1980-2014) climatological wintertime biases in (left) temperature and (right) zonal wind across the eastern Pacific and western North America. Colored curves indicate the biases of the dynamically downscaled simulations. The thick black curve represents the CMIP6 ensemble mean (30 GCMs, 1 realization each), while the gray shading depicts the CMIP6 model spread.

CMIP6 GCMs are generally characterized by the following mean-state biases across this sector of the planet, shown in Fig. 9:

1. **A lower tropospheric instability bias between the surface and 850 hPa:** This bias manifests in lapse rate magnitudes that are $\sim 3^{\circ}\text{C}/\text{km}$ larger in the CMIP6 ensemble mean than in ERA5. The resultant increase in available potential

energy via parcel theory, if realized by parcels that achieve their level of free convection, may lead to increased precipitation relative to ERA5.

2. **A general tropospheric cold bias of around 2°C:** This has consequences for surface temperatures across high terrain (such as the Sierra) and precipitation phase. For the former, many land-surface models (including Noah-MP; used here) use a threshold surface temperature that determines the rain/snow partitioning to classify impacting hydrometeors as rain or snow. As this cooler air impinges on topographic barriers, the surface will thus generally remain cooler than it would otherwise in ERA5. Thus, falling precipitation is more likely to be classified as snow rather than rain. As snow accumulates, an albedo feedback ensues which acts to keep surface temperatures cooler than they would otherwise become in a snow-free environment. For the latter, parcels rising in a cooler atmosphere will be more likely to achieve saturation and initiate nucleation processes (both liquid and ice). This cold bias may therefore increase the precipitation efficiency across the region in downscaled GCMs compared to ERA5.
3. **A westerly zonal wind bias throughout the troposphere that increases with increasing height:** Any lower-tropospheric upslope flow will thus be enhanced, leading to enhanced updraft velocities and increased nucleation within clouds (and thus increased precipitation capabilities). In the CMIP6 mean, the bias is on the order of 0.5 m/s in the lower troposphere and increases to around 2 m/s near the tropopause.
4. **A zonal wind shear bias throughout the troposphere:** Storms that evolve in a sufficiently sheared environment may have a greater longevity as their falling hydrometeors are deposited away from the main updraft. Increased storm lifetimes may act to increase precipitation in dynamically downscaled GCM simulations.

Preliminary results from this evaluation suggest that thermodynamic mean-state GCM biases (relating to temperature, lapse rates, and moisture; bullets 1 and 2 above) are most correlated with dynamically downscaled precipitation biases. Meanwhile, mean-state GCM biases in wind are anticorrelated, except across the Pacific Northwest, where the removal of wind biases are found to improve dynamically downscaled precipitation biases.

As it pertains to the above mean-state biases, CESM2 and ECE are the least biased in tropospheric temperature compared to CNRM and FGOALS, and the lower-tropospheric instability bias in ECE is virtually absent. CESM2 and ECE also have the smallest zonal wind biases in the lower half of the troposphere compared to CNRM and FGOALS. These mean-state biases may begin to explain their relatively smaller precipitation biases compared to CNRM and FGOALS (Fig. 7). Furthermore, the spatiality of the precipitation biases seems to indicate that the mean-state biases are exacerbated by forcing from local topography. Additionally, biases in high-frequency weather-scale winds, temperature, and moisture may be contributing to biases in precipitation. Indeed, even though extensive testing of WRF was conducted to optimize its simulation of weather and climate across the western US (Rahimi et al., 2022), and even though

GCMs were chosen based on how well they simulated the regional synoptics (Task 3 *Memorandum on Evaluating Global Climate Models for Studying Regional Climate Change in California*), large internal GCM biases, characteristic of the greater CMIP6 ensemble, remain, leading to large differences between the downscaled GCMs and PRISM. We postulate that this general behavior, namely hyperactive precipitation, can be expected when downscaling a given CMIP6 GCM across this region using this configuration of WRF.

4. Diversity of future precipitation and temperature changes for WRF projections for this project

We begin by examining the future changes in precipitation and temperature. We intentionally selected GCMs to downscale based on how wet and warm their futures became and ensured that their respective future projections were relatively balanced and unique from each other. Following precipitation and temperature, we examine future changes in other variables from our four dynamically downscaled GCMs.

4.1 Historically evaluated variables

The dynamically downscaled GCMs showcase a diversity of future changes in terms of temperature and precipitation, and these projected changes can locally be vastly different between the parent GCM and its respective downscaled solution. All anomalies in this section are computed as the 2070-2100 climatology minus the 1980-2010 climatology¹. The large-scale GCM signal is generally preserved in downscaling for all GCMs for both the wet and warm seasons (Figures 10 and 11). Additionally, a widely forecast inland-directed gradient to the warming presents in all simulations (both GCM and downscaled), as well as generally maximized warming anomalies during the warm season (Fig. 10). CRNM and ECE seem to warm the most in the future, while FGOALS sees much smaller levels of warming (around 2°C) in the California state mean.

Prominent California landscape features such as the Salton Sea, the Sierra Nevada, and several southern California mountain ranges distinguish the dynamically downscaled products from their parent GCMs as WRF can resolve these geographic features and their subsequent impact on local weather and climate. As a result, locally maximized wet season warming, possibly associated with the snow-albedo feedback, is projected in proximity to California high points in CESM2, CNRM, and ECE, while a more homogeneous warming pattern is simulated in FGOALS. During the warm season, CNRM and ECE see warming of nearly 6°C in the future along the spine of the Sierra; this region only warms by ~4°C in the future in their respective GCM parents. Even the 0.7°-grid spacing ECE GCM showcases large differences with its downscaled counterpart locally, particularly during the wet season.

As with T2MEAN, the large-scale change in PREC is generally preserved in downscaling, and the four GCMs depict a diversity of plausible futures (Figure 11).

¹ The entirety of the CMIP6 historical time period (1980-2014) was considered for bias evaluation purposes. Since, for the climate change calculations, we use the last 30 years of the 21st century in computing the end-century climatology, it made sense to use a 30-year historical reference period in the calculations of the future change signal as opposed to a 35-year historical climatology.

During the wet season, CESM2 and FGOALS universally project a wetter future across California, with the maximum increase in precipitation collocated with California's complex terrain features. Meanwhile, although the ECE and CNRM GCMs simulate future drying across most, if not all, of California, their downscaled counterparts provide a signal of increased heterogeneity with pronounced wetting along the spine of the Sierra in CNRM and other regions of complex terrain. We also see wetting in the northern Central Valley in ECE, a feature that is absent in the parent GCM. For the warm season, differences between the dynamically downscaled simulations and the parent GCMs are more pronounced, and CESM2, CNRM, ECE, and FGOALS all predict a wetter future in the Sierra Nevada. CNRM amplifies the drying of its parent GCM across most of California, with locally maximized drying of 1 mm/d across the northern upslope of the Sierra. It appears that the RCM amplifies the change signal of the parent GCM, and the larger GCM/RCM differences during the warm season may be associated with seasonally weaker large-scale forcing for ascent, which would lessen the impacts of spectral nudging (conducted on the 45-km grid) on the downstream higher resolution WRF products (i.e., 9- and 3-km). Finally, the cooler temperature response across California in CESM2 and especially FGOALS may be the result of offsetting cooling associated with projected increases in precipitation.

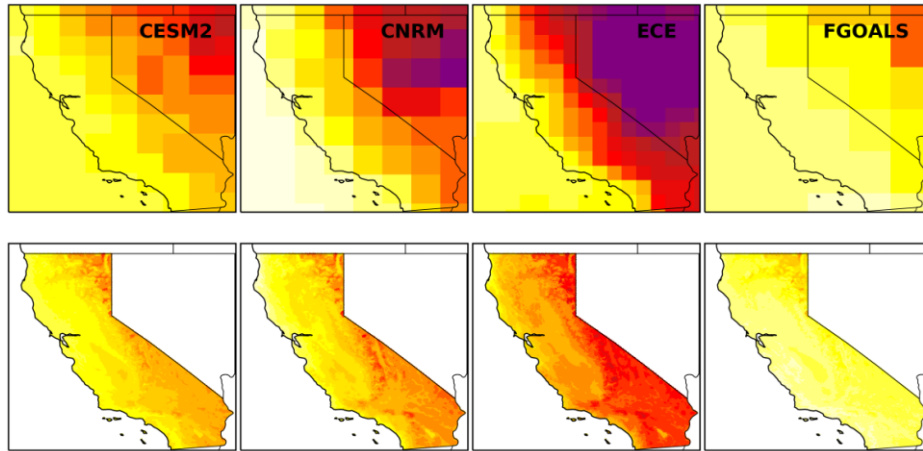
We also find shifts in the distributions of daily T2MEAN and PREC (Figure 12). Across California, an expected warming profile to the distribution is noted, with the weakest (strongest) warming signal simulated in FGOALS (ECE). For PREC meanwhile, simulations project quite different futures for lower-intensity precipitation events (< 10 mm/d), with CESM2 and FGOALS wetting and CNRM and ECE drying. For extreme precipitation rates however (> 100 mm/d), all simulations predict higher-intensity extremes by the end of the 21st century. This predicted wetting of the tail has been forecast in other studies using CESM2 across California (Swain et al., 2018).

4.2 Other variables

Here we examine high resolution future changes in certain variables which cannot be derived physically using any of the other modeling methods in EPC-20-006.

During the wet season, beginning with 10 meter wind speeds and 2 meter vapor pressure deficit (VPD; defined as the difference between the saturation vapor pressure and the vapor pressure), we find a diversity of futures in our downscaled simulations (Figures 13 and 14). VPD increases everywhere, with the maximum increases at lower elevations and away from areas of complex terrain, indicating that surface evaporation will preferentially increase at these locations in the future. Future increases in VPD generally increase with south and eastward extend across the state, and FGOALS seems to be an outlier in terms of wet season VPD anomalies, which are smaller in magnitude relative to CESM2, CNRM, and ECE. Wind speeds on the other hand generally decrease in the future in all simulations, and the decreases tend to be larger over regions of complex terrain and at higher elevations. Diversity in the future change signal presents for winds offshore; CNRM, ECE, and FGOALS all simulate weakening future winds, while CESM2 simulates slight strengthening.

Wet season future changes in T2MEAN



Warm season future changes in T2MEAN

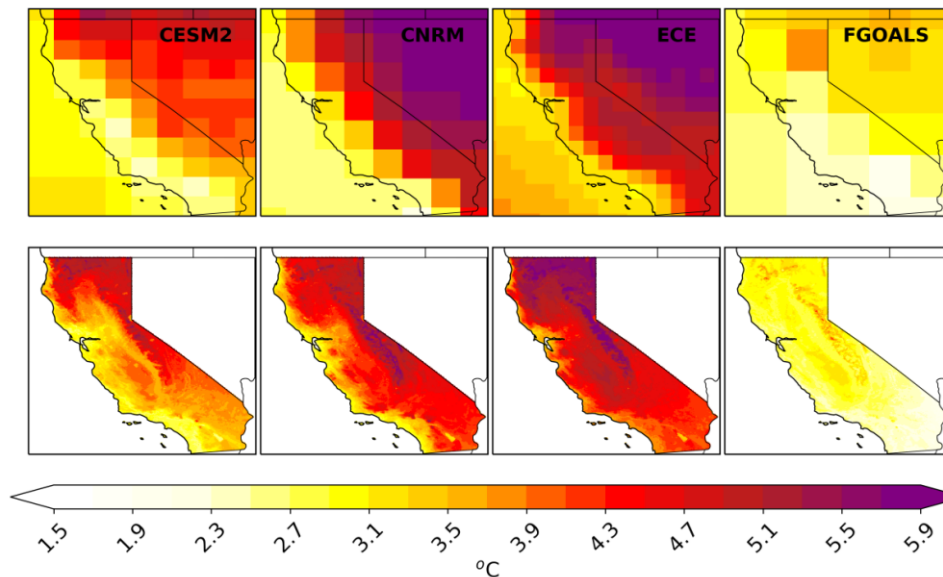


Figure 10. Future anomalies in temperature across California for the dynamically downscaled GCMs during the wet and warm seasons. The top row is the native GCM change and the bottom row is the change in 3 km WRF data. Anomalies are computed as the 2070-2100 means minus the 1980-2010 mean.

During the warm season, VPD increases are larger relative to the wet season, with again a diversity of future evaporative potential with the same spatiality of the change as in the wet season. FGOALS again generally simulates the smallest increase in VPD values, while CNRM and especially ECE see locally maximized future increases in VPD across the Central Valley (ECE and CNRM warm the most comparatively). For winds, striking consistency in the downscaled result is noted across several regions of California:

1. Winds are weaker in the future across the spine of the Sierra
2. Winds are weaker in the future off the California coast

3. Winds are stronger in the future across portions of the Sierra Madre
4. Winds are stronger in the future across the San Francisco Bay area and inner channel. This is probably due to a strong projected eastward-directed gradient to the warming pattern, with stronger inland warming, yielding an anomalous pressure gradient force. Increased wind speeds manifest as the mass response is funneled through the channel via Bernoulli effects.
5. Winds are weaker in the future across the San Gabriel

Furthermore, winds strengthen in the future in the San Bernadino mountains in CESM2 and CNRM but weaken in ECE and FGOALS.

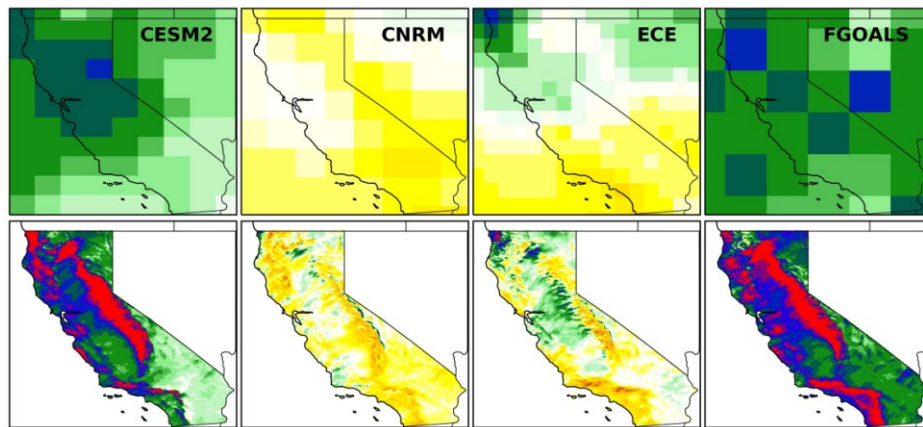
5. Data uses in EPC-20-006

The WRF data will be used for purposes of the EPC-20-006 project; specifically by the statistical downscaling (Task 5) and hydrology (Task 6) teams.

WRF data will be bias corrected before use by the statistical downscaling team as training data in LOCA, their statistical downscaling product. This marriage of WRF and LOCA births a novel hybrid downscaling framework and is a cornerstone feature of EPC-20-006. Additionally, WRF hourly outputs, including precipitation and temperature, are being used to drive continuous, calibrated hydrology experiments offline.

An important advance that is provided by the EPC-20-006 project is that it develops two data sets by applying two different downscaling approaches. End users are given the option of deciding which data is best suited for their particular applications. The dynamically downscaled projections that are described in this memo and in the first Task 4 memo contain physically consistent downscaled data with high temporal resolution: 6 hourly for all output and up to hourly for some variables. The dynamical downscaled data is used in the EPC-20-006 project in training the statistical downscaling (resulting in the LOCA hybrid data), which is more computationally economical than the dynamical downscaling and thus able to produce projections from many global climate models under different possible greenhouse gas and socioeconomic scenarios. Training from dynamical model simulations over the 21st Century averts the traditional "stationarity assumption" that climate patterns in the past will also be the same in the future. However, as described in this memo, the dynamical downscaling simulations have large biases for some variables. These biases will be of concern to some users, so the LOCA hybrid data, which is daily and includes fewer variables, will be biased corrected. Depending on the needs of the analysis, the dynamical or hybrid downscaled data may be the best suited for certain end-uses.

Wet season future changes in PREC



Warm season future changes in PREC

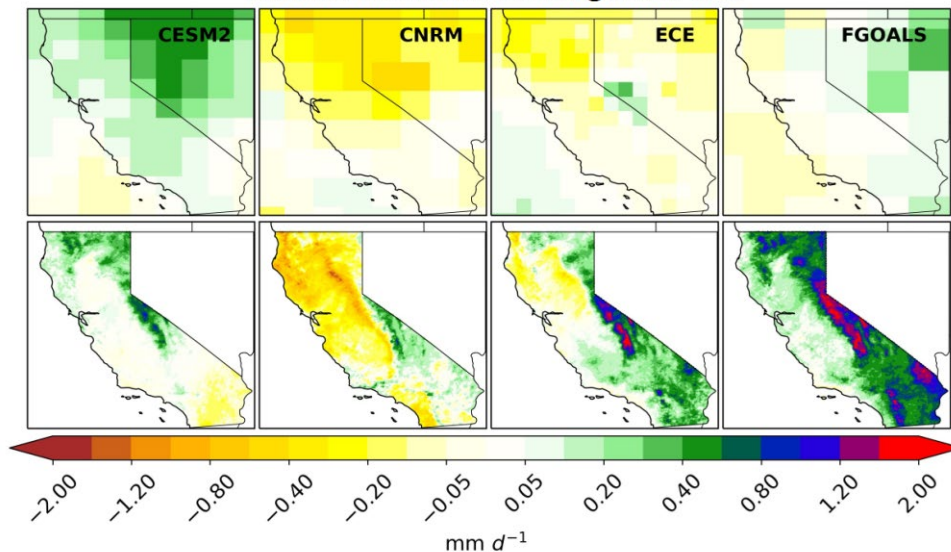


Figure 11. Same as in Fig. 10 but for PREC.

6. Data access

To recap, 6-hourly hourly, and daily WRF data from the discussed simulations (see the *Memo on the Development and Availability of Dynamically Downscaled Projections Using WRF*) on a 45-km grid that covers western North America, a 9-km grid that covers the entirety of the western United States, and a 3-km convective-permitting grid with California-wide coverage.

Data discussed delivered to CEC in this task, Task 4, as well as data from the larger ensemble delivered for other research grants, are located in an open data bucket on Amazon S3. See bucket details at <https://registry.opendata.aws/wrf-cmip6/>. Amazon provides open-source software that allows for free and fast data transfers from S3 to your local devices via the Amazon Web Service Command Line Interface (AWS CLI). Specifically, Task 4 WRF data can be accessed on S3 at:

1. **ERA5 downscaled reanalysis**– s3://wrf-cmip6-noversioning/downscaled_products/reanalysis/era5/
2. **CESM2 downscaled GCM** – s3://wrf-cmip6-noversioning/downscaled_products/gcm/cesm2_r11i1p1f1_historical/ and s3://wrf-cmip6-noversioning/downscaled_products/gcm/cesm2_r11i1p1f1_ssp370/
3. **CNRM-ESM2-1 downscaled GCM** – s3://wrf-cmip6-noversioning/downscaled_products/gcm/cnrm-esm2-1_r1i1p1f2_historical/ and s3://wrf-cmip6-noversioning/downscaled_products/gcm/cnrm-esm2-1_r1i1p1f2_ssp370/
4. **EC-Earth3-Veg downscaled GCM** – s3://wrf-cmip6-noversioning/downscaled_products/gcm/ec-earth3-veg_r1i1p1f1_historical/ and s3://wrf-cmip6-noversioning/downscaled_products/gcm/ec-earth3-veg_r1i1p1f1_ssp370/
5. **FGOALS-g3 downscaled GCM** – s3://wrf-cmip6-noversioning/downscaled_products/gcm/fgoals-g3_r1i1p1f1_historical/ and s3://wrf-cmip6-noversioning/downscaled_products/gcm/fgoals-g3_r1i1p1f1_ssp370/

All other dynamically downscaled GCM data can be found in s3://wrf-cmip6-noversioning/downscaled_products/gcm/.

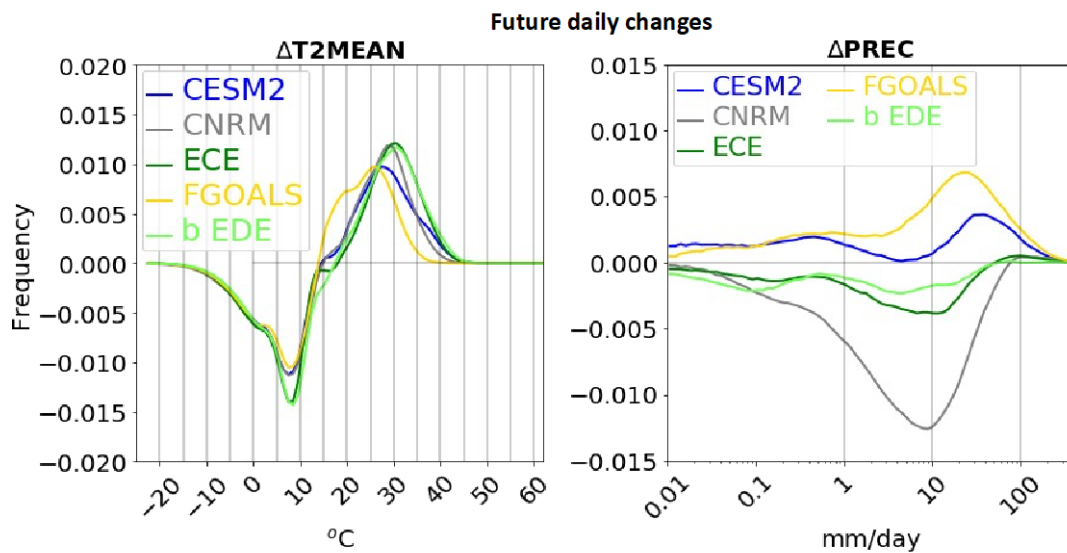


Figure 12. Future changes in the distribution of (left) T2MEAN and (right) PREC across the entire state of California. Each distribution is calculated by considering the full annual cycle, binning daily quantities for all California gridcells in the historical (1980-2010) and future (2070-2100) periods. The distribution differences are then computed.

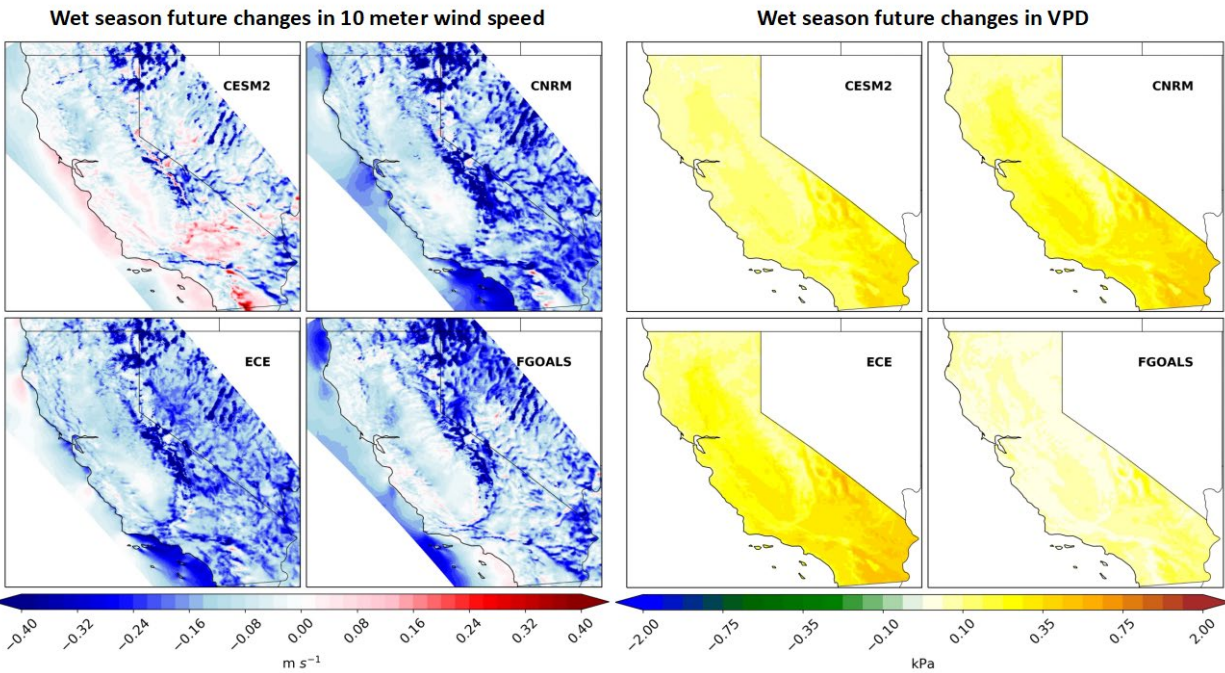


Figure 13. Future climatological changes in (left) 10 m wind speed and (right) vapor pressure deficit (VPD) during the wet season (October to March). As in previous figures, anomalies are computed as the 2070-2100 means minus the 1980-2010 mean. Different from previous figures in which all non-California gridcells were masked, we included usable gridcells outside of the state here for winds due to recent interest in predicting offshore winds.

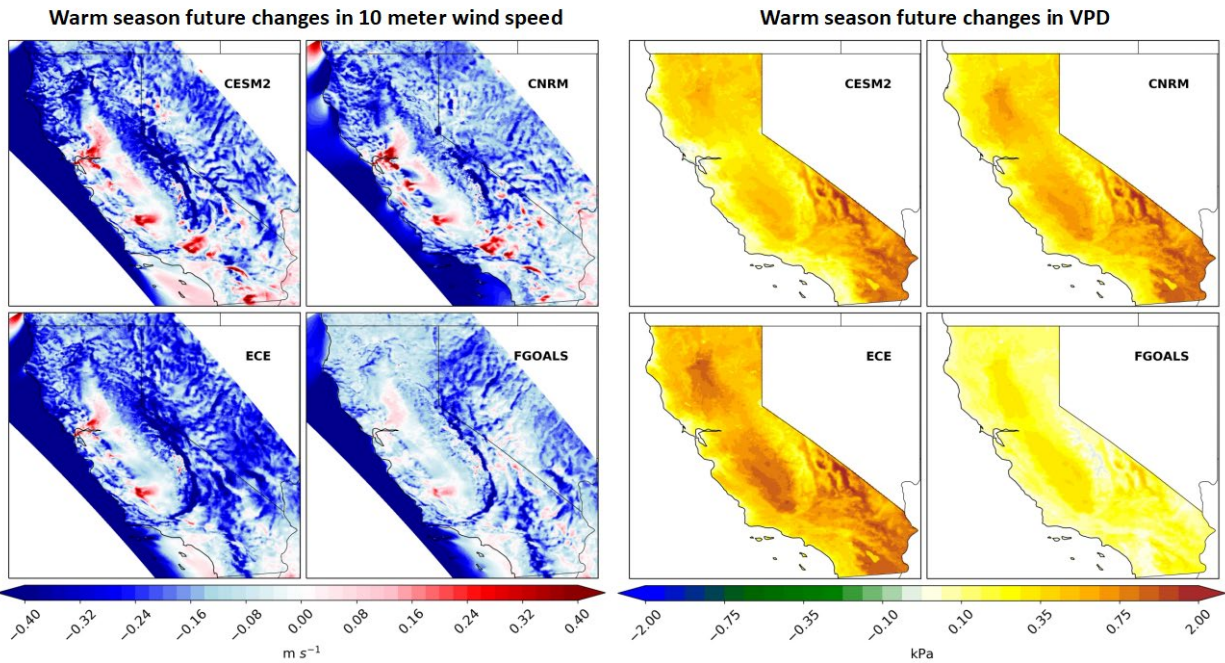


Figure 14. Same as in Fig. 13, but for the warm season (June through September).

Find previous memos referend here:

Krantz, W., Pierce, D., Goldenson, N., and Cayan, D. (2021). Projected climate, heat waves and extreme weather for the 21st Century, https://www.energy.ca.gov/sites/default/files/2022-09/20220907_CDAWG_MemoEvaluating_GCMs_EPC-20-006_Nov2021-ADA.pdf

Rahimi, S. (2022). Memo on the development and availability of dynamical downscaled projections using WRF, https://www.energy.ca.gov/sites/default/files/2022-09/20220907_CDAWG_MemoDynamicalDownscaling_EPC-20-006_May2022-ADA.pdf

7. References

- Bruyère, C. L., Done, J. M., Holland, G. J., & Fredrick, S. (2014). Bias corrections of global models for regional climate simulations of high-impact weather. *Climate Dynamics*, 43(7), 1847–1856. <https://doi.org/10.1007/s00382-013-2011-6>
- Cai, X., Yang, Z.-L., David, C. H., Niu, G.-Y., & Rodell, M. (2014). Hydrological evaluation of the Noah-MP land surface model for the Mississippi River Basin. *Journal of Geophysical Research: Atmospheres*, 119(1), 23–38. <https://doi.org/10.1002/2013JD020792>
- Coppola, E., Sobolowski, S., Pichelli, E., Raffaele, F., Ahrens, B., Anders, I., et al. (2020). A first-of-its-kind multi-model convection permitting ensemble for investigating convective phenomena over Europe and the Mediterranean. *Climate Dynamics*, 55(1), 3–34. <https://doi.org/10.1007/s00382-018-4521-8>
- Coppola, E., Nogherotto, R., Ciarlo, J. M., Giorgi, F., van Meijgaard, E., Kadyrov, N., et al. (2021). Assessment of the European Climate Projections as Simulated by the Large EURO-CORDEX Regional and Global Climate Model Ensemble. *Journal of Geophysical Research: Atmospheres*, 126(4), e2019JD032356. <https://doi.org/10.1029/2019JD032356>
- Hersbach, H., Bell, B., Berrisford, P., Hirahara, S., Horányi, A., Muñoz-Sabater, J., et al. (2020). The ERA5 global reanalysis. *Quarterly Journal of the Royal Meteorological Society*, 146(730), 1999–2049. <https://doi.org/10.1002/qj.3803>
- Huang, X., Swain, D. L., Walton, D. B., Stevenson, S., & Hall, A. D. (2020). Simulating and Evaluating Atmospheric River-Induced Precipitation Extremes Along the U.S. Pacific Coast: Case Studies From 1980–2017. *Journal of Geophysical Research: Atmospheres*, 125(4), e2019JD031554. <https://doi.org/10.1029/2019JD031554>
- Iacono, M. J., Delamere, J. S., Mlawer, E. J., Shephard, M. W., Clough, S. A., & Collins, W. D. (2008). Radiative forcing by long-lived greenhouse gases: Calculations with the AER radiative transfer models. *Journal of Geophysical Research: Atmospheres*, 113(D13). <https://doi.org/10.1029/2008JD009944>
- Komurcu, M., Emanuel, K. A., Huber, M., & Acosta, R. P. (2018). High-Resolution Climate Projections for the Northeastern United States Using Dynamical Downscaling at Convection-Permitting Scales. *Earth and Space Science*, 5(11), 801–826. <https://doi.org/10.1029/2018EA000426>
- Lanzante, J. R., Dixon, K. W., Nath, M. J., Whitlock, C. E., & Adams-Smith, D. (2018). Some Pitfalls in Statistical Downscaling of Future Climate. *Bulletin of the American Meteorological Society*, 99(4), 791–803. <https://doi.org/10.1175/BAMS-D-17-0046.1>

- Liu, C., Ikeda, K., Thompson, G., Rasmussen, R., & Dudhia, J. (2011). High-Resolution Simulations of Wintertime Precipitation in the Colorado Headwaters Region: Sensitivity to Physics Parameterizations. *Monthly Weather Review*, *139*(11), 3533–3553. <https://doi.org/10.1175/MWR-D-11-00009.1>
- Liu, C., Ikeda, K., Rasmussen, R., Barlage, M., Newman, A. J., Prein, A. F., et al. (2017). Continental-scale convection-permitting modeling of the current and future climate of North America. *Climate Dynamics*, *49*(1), 71–95. <https://doi.org/10.1007/s00382-016-3327-9>
- Lundquist, J., Hughes, M., Gutmann, E., & Kapnick, S. (2019). Our Skill in Modeling Mountain Rain and Snow is Bypassing the Skill of Our Observational Networks. *Bulletin of the American Meteorological Society*, *100*(12), 2473–2490. <https://doi.org/10.1175/BAMS-D-19-0001.1>
- Mitchell, D. L., Ivanova, D., Rabin, R., Brown, T. J., & Redmond, K. (2002). Gulf of California Sea Surface Temperatures and the North American Monsoon: Mechanistic Implications from Observations. *Journal of Climate*, *15*(17), 2261–2281. [https://doi.org/10.1175/1520-0442\(2002\)015<2261:GOCSSST>2.0.CO;2](https://doi.org/10.1175/1520-0442(2002)015<2261:GOCSSST>2.0.CO;2)
- Morrison, H., & Milbrandt, J. (2015). Parameterization of Cloud Microphysics Based on the Prediction of Bulk Ice Particle Properties. Part I: Scheme Description and Idealized Tests. *Journal of the Atmospheric Sciences*, *72*, 287–311. <https://doi.org/10.1175/JAS-D-14-0065.1>
- Niu, G.-Y., Yang, Z.-L., Mitchell, K. E., Chen, F., Ek, M. B., Barlage, M., et al. (2011). The community Noah land surface model with multiparameterization options (Noah-MP): 1. Model description and evaluation with local-scale measurements. *Journal of Geophysical Research: Atmospheres*, *116*(D12). <https://doi.org/10.1029/2010JD015139>
- PRISM Climate Group, Oregon State University, <https://prism.oregonstate.edu>, data created 4 Feb 2014, accessed 16 Dec 2021.
- Rahimi, S., Krantz, W., Lin, Y.-H., Bass, B., Goldenson, N., Hall, A., et al. (2022). Evaluation of a Reanalysis-Driven Configuration of WRF4 Over the Western United States From 1980 to 2020. *Journal of Geophysical Research: Atmospheres*, *127*(4), e2021JD035699. <https://doi.org/10.1029/2021JD035699>
- Rasmussen, R., Ikeda, K., Liu, C., Gochis, D., Clark, M., Dai, A., et al. (2014). Climate Change Impacts on the Water Balance of the Colorado Headwaters: High-Resolution Regional Climate Model Simulations. *Journal of Hydrometeorology*, *15*(3), 1091–1116. <https://doi.org/10.1175/JHM-D-13-0118.1>
- Skamarock, C., Klemp, B., Dudhia, J., Gill, O., Liu, Z., Berner, J., et al. (2019). A Description of the Advanced Research WRF Model Version 4. <https://doi.org/10.5065/1dfh-6p97>
- Swain, D. L., Langenbrunner, B., Neelin, J. D., & Hall, A. (2018). Increasing precipitation volatility in twenty-first-century California. *Nature Climate Change*, *8*(5), 427–433. <https://doi.org/10.1038/s41558-018-0140-y>
- Tiedtke, M. (1989). A Comprehensive Mass Flux Scheme for Cumulus Parameterization in Large-Scale Models. *Monthly Weather Review*, *117*(8), 1779–1800. [https://doi.org/10.1175/1520-0493\(1989\)117<1779:ACMFSF>2.0.CO;2](https://doi.org/10.1175/1520-0493(1989)117<1779:ACMFSF>2.0.CO;2)

- Wang, J., & Kotamarthi, V. R. (2015). High-resolution dynamically downscaled projections of precipitation in the mid and late 21st century over North America. *Earth's Future*, 3(7), 268–288. <https://doi.org/10.1002/2015EF000304>
- Wang, J., Han, Y., Stein, M. L., Kotamarthi, V. R., & Huang, W. K. (2016). Evaluation of dynamically downscaled extreme temperature using a spatially-aggregated generalized extreme value (GEV) model. *Climate Dynamics*, 47(9), 2833–2849. <https://doi.org/10.1007/s00382-016-3000-3>
- Zhang, C., Wang, Y., & Hamilton, K. (2011). Improved Representation of Boundary Layer Clouds over the Southeast Pacific in ARW-WRF Using a Modified Tiedtke Cumulus Parameterization Scheme. *Monthly Weather Review*, 139(11), 3489–3513. <https://doi.org/10.1175/MWR-D-10-05091.1>
- Zobel, Z., Wang, J., Wuebbles, D. J., & Kotamarthi, V. R. (2017). High-Resolution Dynamical Downscaling Ensemble Projections of Future Extreme Temperature Distributions for the United States. *Earth's Future*, 5(12), 1234–1251. <https://doi.org/10.1002/2017EF000642>
- Zobel, Z., Wang, J., Wuebbles, D. J., & Kotamarthi, V. R. (2018). Evaluations of high-resolution dynamically downscaled ensembles over the contiguous United States. *Climate Dynamics*, 50(3–4), 863–884. <https://doi.org/10.1007/s00382-017-3645-6>

Appendix I. Additional WRF projections across the western United States

In this section, we advertise the greater ensemble of GCMs, of which the four CEC-funded WRF projections are a small part. We proceed by stating that, although these simulations are not funded by CEC, we support their use following their publication. They are also located in the open data bucket on Amazon S3. See bucket details at <https://registry.opendata.aws/wrf-cmip6/>.

Initially, 9 different GCM (including the 4 CEC WRF projections) are downscaled 9-km across the western United States. For CESM2, two additional simulations were conducted for the SSP2-4.5 and SSP5-8.5 emissions pathways. Future changes in cumulative water year precipitation for our entire ensemble are shown in Figure 15. Additionally, each of the SSP3-7.0 GCMs are dynamically downscaled as a pair of simulations, one using standard dynamical downscaling, and a second which sees a mean-state bias correction applied to the GCM inputs before WRF downscaling (a pre-downscaling bias correction) following Bruyère et al. (2014). The reference dataset used for bias correction is the ERA5 reanalysis, and the bias correction is only applied to the 3-dimensional horizontal winds, temperature, and specific humidity, as well as surface pressure, mean sea-level pressure, and sea-surface temperatures. The mean-state bias correction is applied monthly. In summary, a total of 20 simulations are dynamically downscaled to 9-km. In addition to the four 3-km simulations provided to CEC, and fifth 3-km experiment was completed across California from 1980-2100 for ECE with a pre-downscaling bias correction (b ECE). A summary of all total experiments is given in Figure 16.

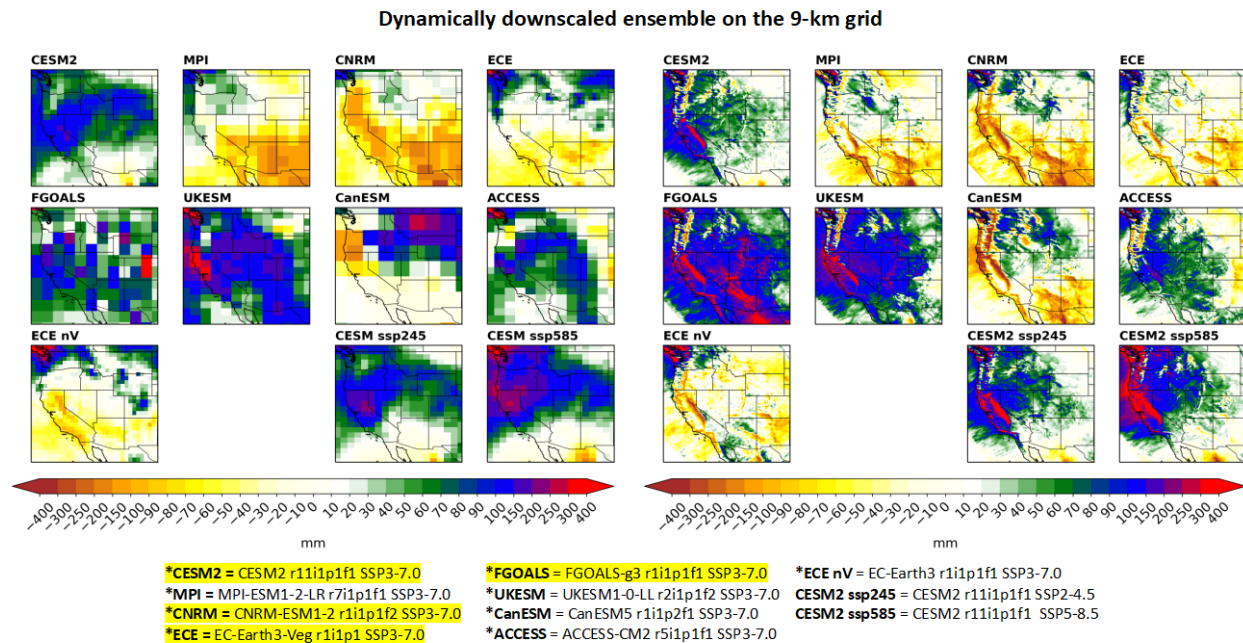


Figure 15. Future (2070-2100 mean) minus historical (1980-2100) differences in cumulative water year precipitation for parent GCMs (left) and their downscaled counterparts (right) within our full ensemble. Yellow highlighted GCMs are those promised to CEC, while asterisks indicate that GCMs have a companion simulation in which a mean-state bias correction was applied prior to downscaling. For non-SSP3-7.0 simulations, we include the associated SSPs in the labeling. This chart is valid as of 21 October 2022.

While the climate change signal of cumulative water year precipitation is quite variable across our downscaled GCM ensemble, we note three items:

1. The large-scale change signal in precipitation from the parent GCM continues to be preserved following dynamical downscaling, regardless of whether pre-downscaling bias correction is used (Figure 15).
2. The change signal is generally quite similar between the non-bias corrected and the bias corrected downscaled experiments, although we do note some large local differences in the change signal (e.g., CNRM across the Sierra; Figure 17)
3. There is a strong landscape heterogeneity in the expression of the downscaled climate change signal that cannot be resolved in the native GCM.

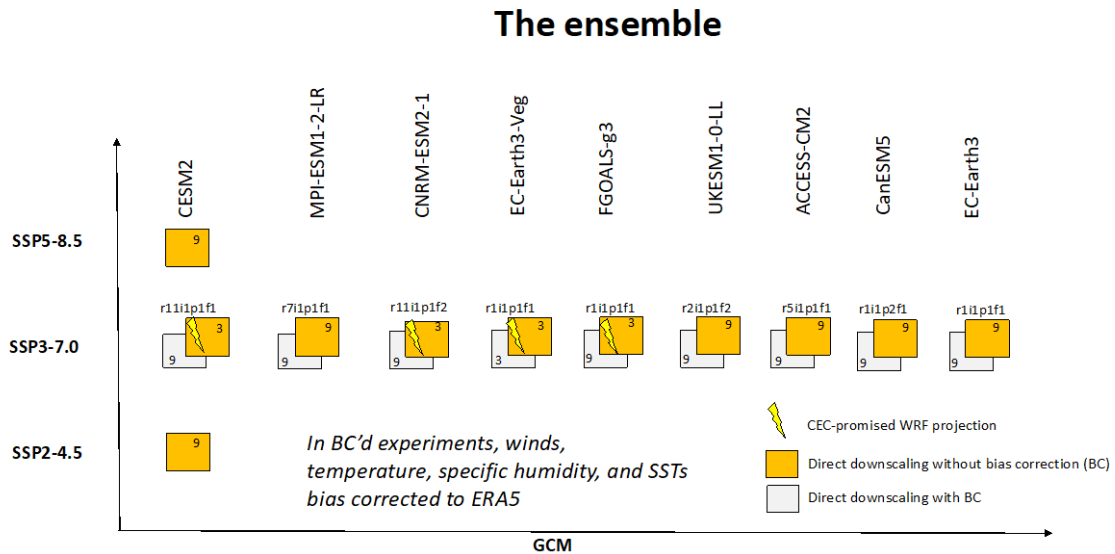


Figure 16. Graphic showing where the CEC WRF projections (denoted by the lightning bolts) fall within the larger 20-member ensemble. The numbers in each square denote the highest resolution grid downscaled to. For example, a 3 indicates that the GCM has been downscaled to 45-, 9-, and 3-km. Here, BC is an acronym for pre-downscaling bias correction.

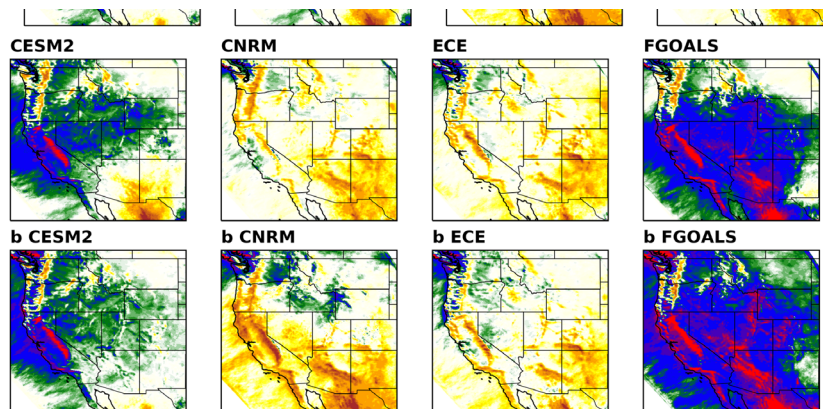


Figure 17. Future (2070-2100 mean) minus historical (1980-2100) differences in cumulative water year precipitation for experiments in which pre-downscaling bias correction was and was not applied on the 9-km western US grid.

Finally, we briefly examine the effects of pre-downscaling bias correction on the downscaled GCMs at 9-km grid spacings. Figure 18 shows the historical daily

climatologies of precipitation and its future change at SNOTEL sites across various western US subregions shown in Fig. 2.

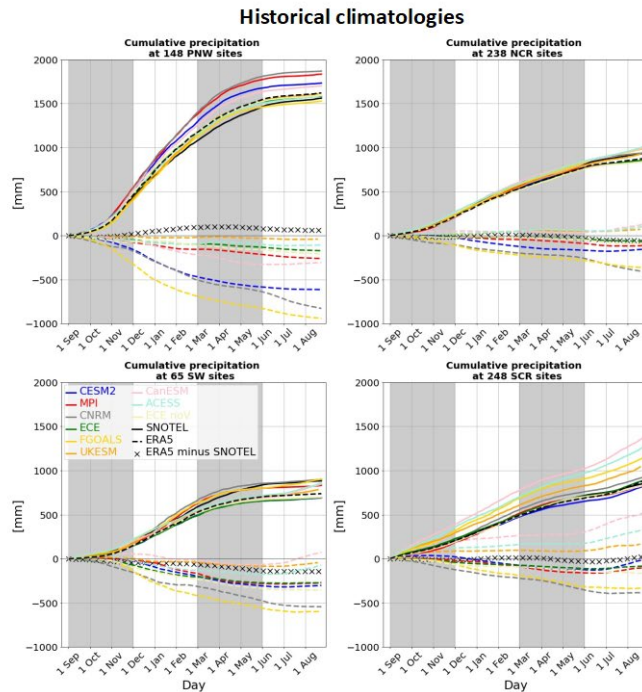


Figure 18 Cumulative precipitation climatologies for the bias corrected experiments (solid lines) at SNOTEL sites across the southwest (SW) south-central Rockies (SCR), north-central Rockies (NCR), and the Pacific Northwest (PNW) regions (see Fig. 2). The black dashed curve shows the ERA5 climatology, while the hatching shows the differences between ERA5 and SNOTEL (positive values = wetter than observed). The dashed lines in the show the BC'd minus the non-BC'd differences in cumulative precipitation for the downscaled GCMs.

High-level takeaways from Figs. 18 and 19 include:

1. For the historical period (Fig. 18), bias corrected (BC'd) experiments are generally drier than their non-BC'd counterparts in terms of their cumulative precipitation as indicated by the dashed curves for each GCM denoting the cumulative difference between the BC'd and non-BC'd experiments (negative means that the BC'd experiments are drier). We also note the small differences between ERA5 and SNOTEL observations (hatch scatter).
2. Generally, biases in cumulative precipitation are reduced as the result of the pre-downscaling bias correction, and GCM results are more like ERA5 results. In some cases, however, drying of the climatologies increases the bias (e.g., across the NCR in MPI).
3. Even after the removal of mean-state biases and subsequent drying of the WRF solution, large biases can remain (e.g., FGOALS in the PNW and the SCR), possibly attributable to higher-frequency biases which are not removed from the GCM inputs. This issue could also be due to an assumed decoupling between the mean-state and deviations from the mean-state in our adopted bias correction approach.

- Bias correction generally preserves the sign of the change signal (Fig. 19). Exceptions to this include MPI and CNRM across the SCR; however, we note that the change signal in cumulative precipitation across these regions is relatively small.
- For the single simulation for which multiple emissions scenarios were downscaled (CESM2), the change signal modification because of bias correction is generally much smaller than the modification associated with changing emissions scenarios. We emphasize that this conclusion can only be applied to CESM2 and may not necessarily hold for other GCMs.

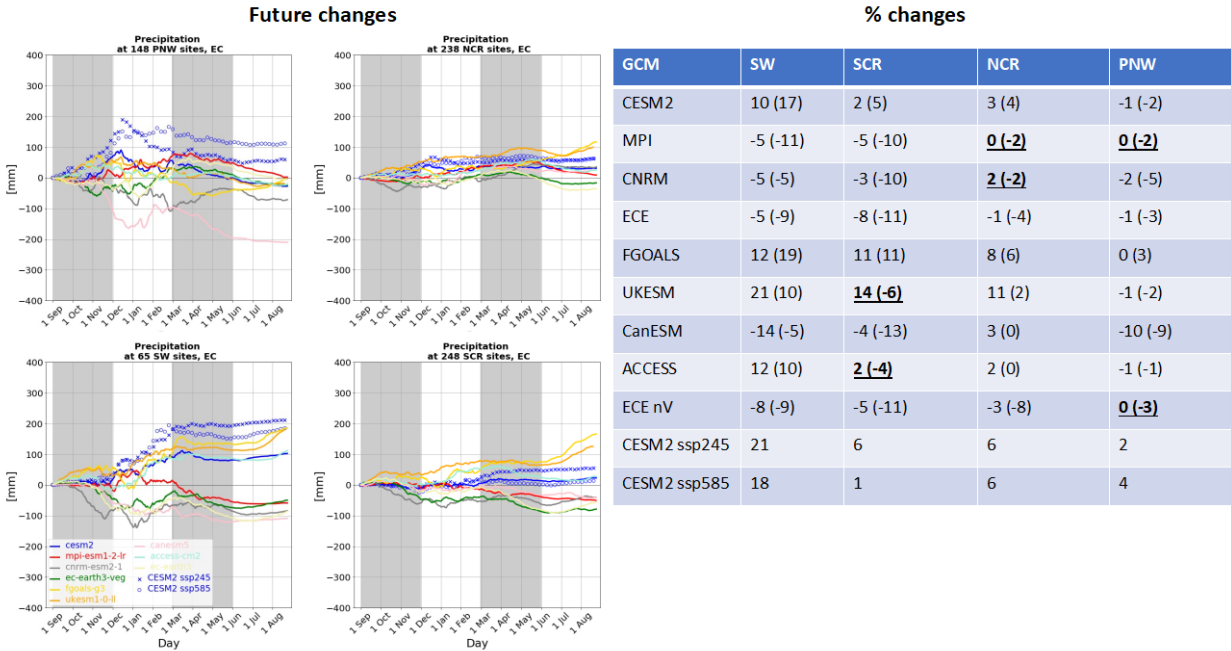


Figure 19. (left) Future changes in cumulative annual precipitation for the non-BC'd experiments and (right) percent changes relative to the historical period for the non-bias corrected experiments. Bias-corrected experimental percent changes are also given in parentheses. The historical (future) period encompasses the 1980-2010 (2070-2100) period.